Poster presented at the
11th Cambridge Workshop on
Cool Stars, Stellar Systems and the Sun
October 4-8, 1999, Puerto de la Cruz, Tenerife, Spain

Numerical Simulations of Surface Convection in Stars with Various Radii

Bernd Freytag

Astronomical Observatory, NBIfAFG, Juliane Maries Vej 30,
DK-2100 Copenhagen East, Denmark, [BF@astro.ku.dk]

Abstract

Based on detailed 2D numerical radiation hydrodynamics calculations of time-dependent compressible convection, the dynamics, spatial scales, and thermal structure of the convective surface layers of different stars with a large range of surface gravities/diameters have been studied.

The characteristic size of the granulation scales well with the pressure scale height at the top of the convection zone. Stars with radiatively dominated weak convection have a larger proportionality factor.

Extrapolation from the findings about White Dwarfs, main-sequence stars, and giants towards red supergiants leads to the conclusion that supergiant stars are covered by only a few granules. First preliminary results from a 3D simulation of such a star are presented.

1 Numerical simulations

Based on 2D numerical radiation hydrodynamics calculations of time-dependent compressible convection, a variety of stellar surface convection zones has been studied. The equation of state accounts for the ionization of H and He (if present). The non-local equation of radiative energy transport is solved along a number of representative rays, assuming LTE. Grey or frequency-dependent opacities can be used (for details see Ludwig, Jordan, Steffen, 1994, A&A 284, 105).

Models with solar-like deep convection zones need a sophisticated open lower boundary condition that allows the free in- and outflow of material. In stars (e.g. A type stars or DA White Dwarfs near the ZZ Ceti instability strip) where the efficient radiative energy transport prohibits efficient adiabatic convection, the convection zones are shallow and can be completely included inside the computational volume and the lower boundary can be closed.

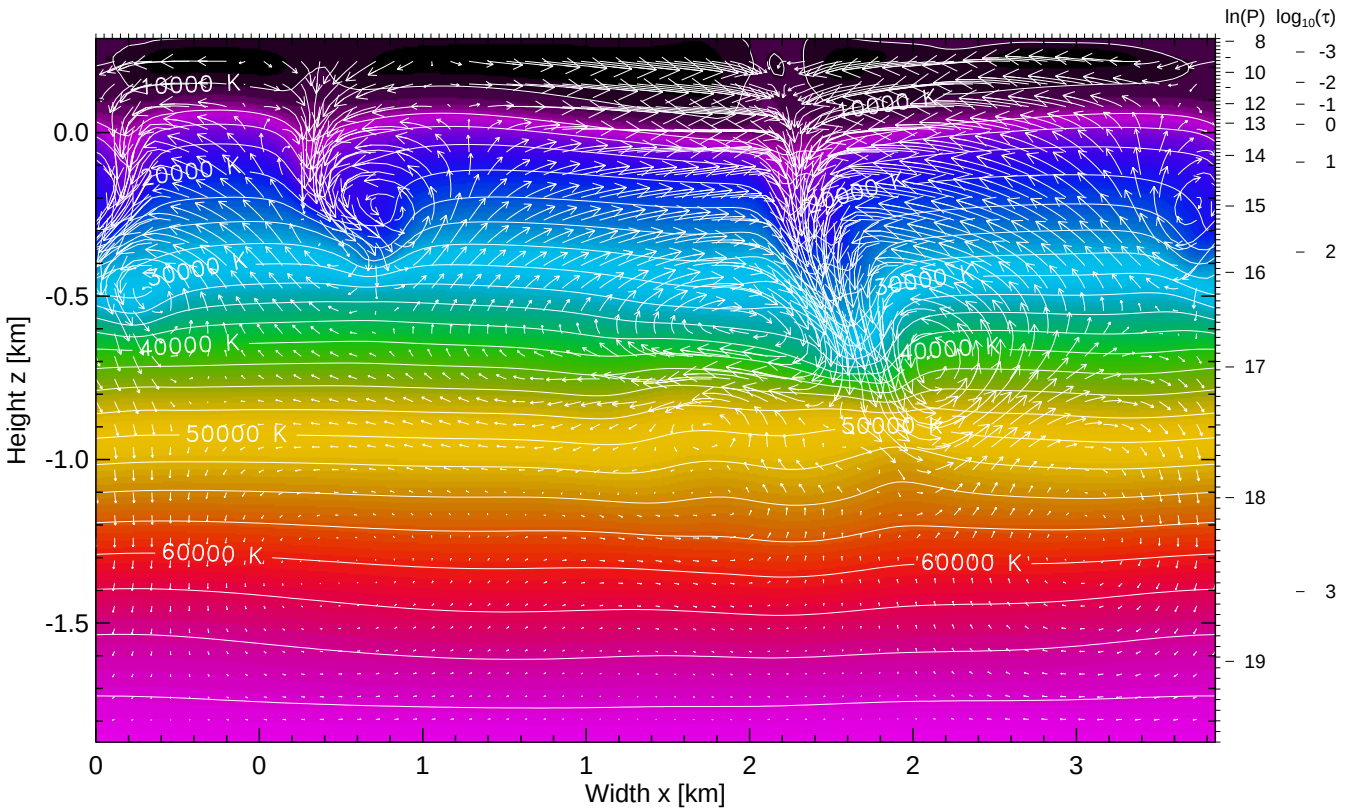

Figure 1: Snapshot of a DA White Dwarf model (zt122g83n2) with $T_{\rm eff}$=12 200 K, log$g$=8.30, pure hydrogen, t=5.6 s, 138×107 grid points, $v_{\rm max}$∼17.4 km/s, $F_{h,\rm max}$∼0.7 $\sigma {T_{\rm eff}}^4$. The complete convection zone including the two overshoot regions is contained in the computational volume.

2 Flow fields

Typical examples of flow patterns are presented in Figs. 1 to 6. The velocity field is indicated by short pseudo-streamlines. Contour lines and colour indicate the temperature T, small tick marks at the top and the right show the positions of the computational grid points. Two columns at the right show horizontally averaged quantities: the natural logarithm of the mean gas pressure and the logarithm of the optical depth. The origin of the height scale on the left corresponds to the layer with $\log \tau = 0$. The height z is counted upward. The lower boundary is open for the solar-type models. The lateral boundary conditions are periodic. Grey opacities are used.

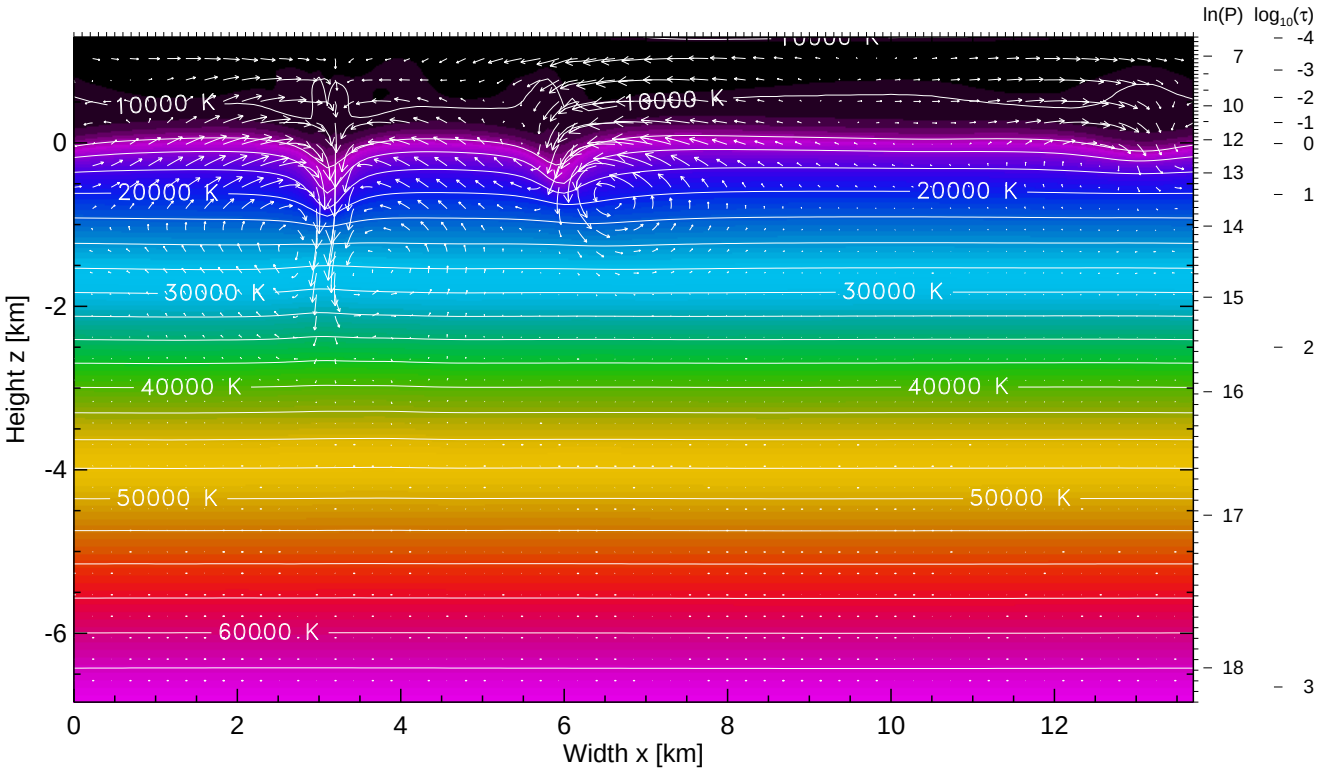

Figure 2: Snapshot of a DA White Dwarf model (zt122g77n1) with $T_{\rm eff}$=12 200 K, log$g$=7.70, pure hydrogen, t22.3 s, 138×91 grid points, $v_{\rm max}$∼15.8 km/s, $F_{h,\rm max}$∼0.11 $\sigma T_{\rm eff}{}^4$. The complete convection zone including the two overshoot regions is contained in the computational volume.

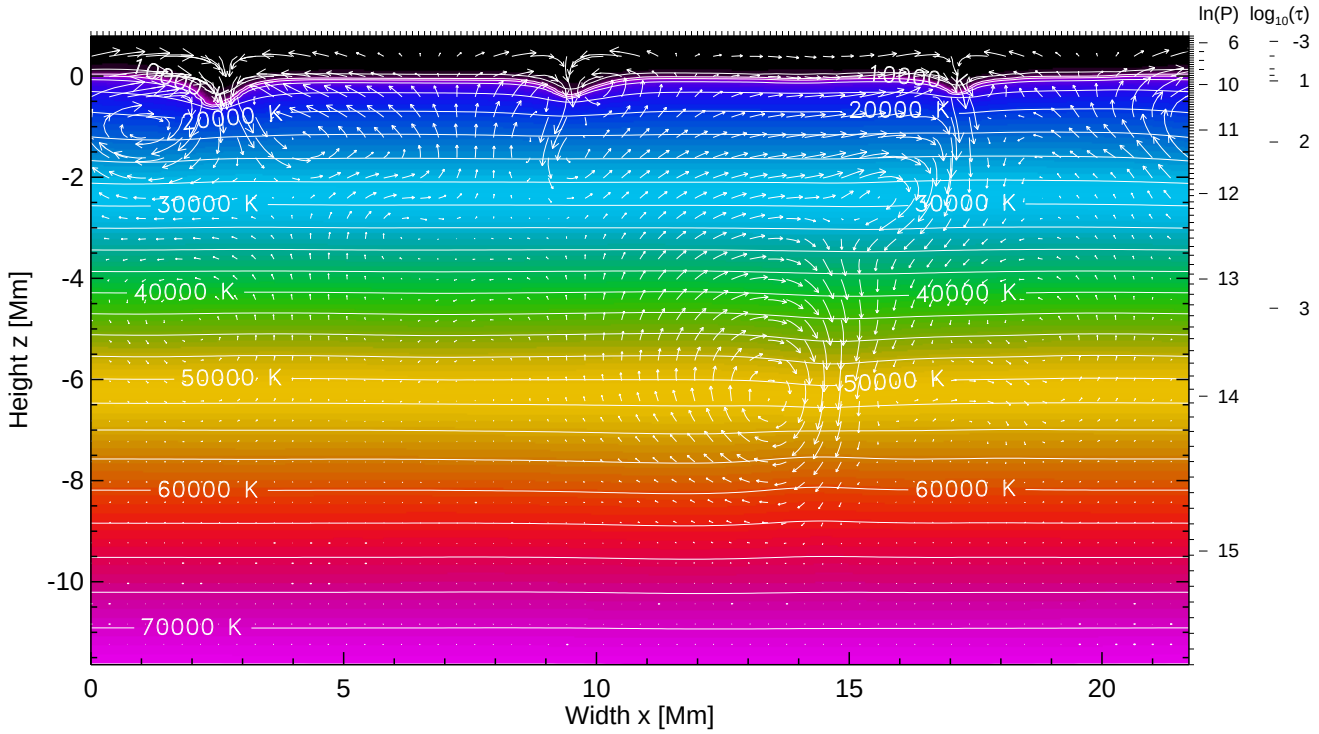

Figure 3: Snapshot of a main-sequence A star model (at80g44n7) with $T_{\rm eff}$=8 000 K, log$g$=4.40, solar metallicity, t=14 000 s, 182×95 grid points, $v_{\rm max}$∼13.6 km/s, $F_{h,{\rm max}}$∼0.15 $\sigma {T_{\rm eff}}^4$. Two connected convectively unstable regions are contained in the computational volume.

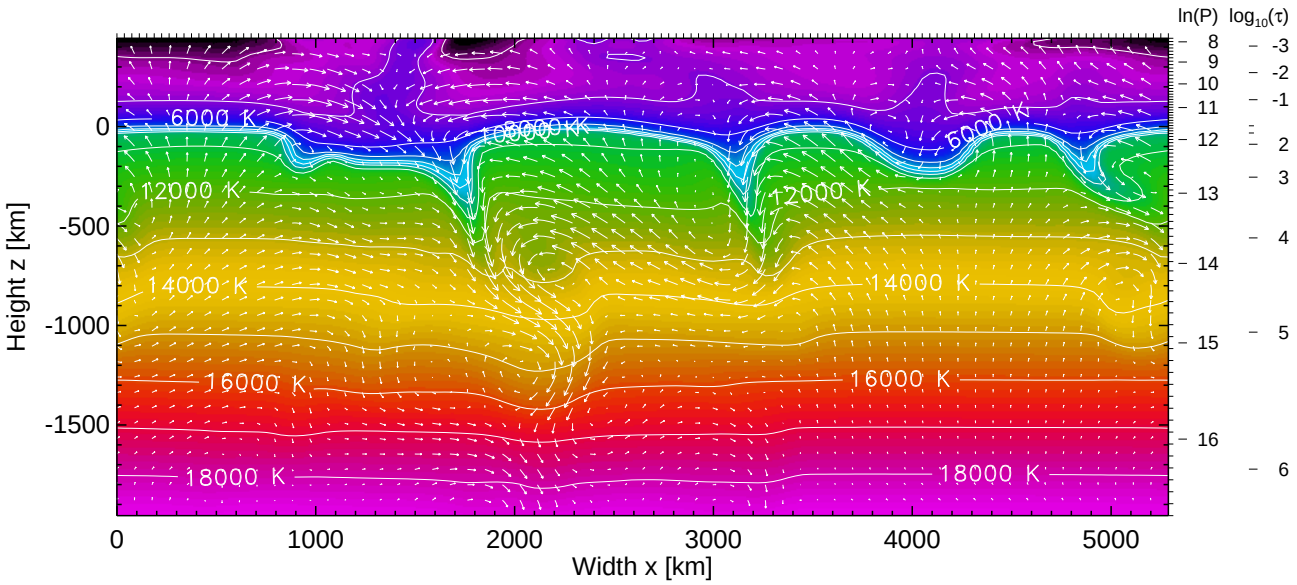

Figure 4: Snapshot of a solar model (gt57g44n9) with $T_{\rm eff}$=5 770 K, log$g$=4.44, solar metallicity, t=67600 s, 142×79 grid points, $v_{\rm max}$∼7.6 km/s, $F_{h,{\rm max}}$∼1 $\sigma {T_{\rm eff}}^4$. Only the upper part of the convection zone is contained in the computational volume.

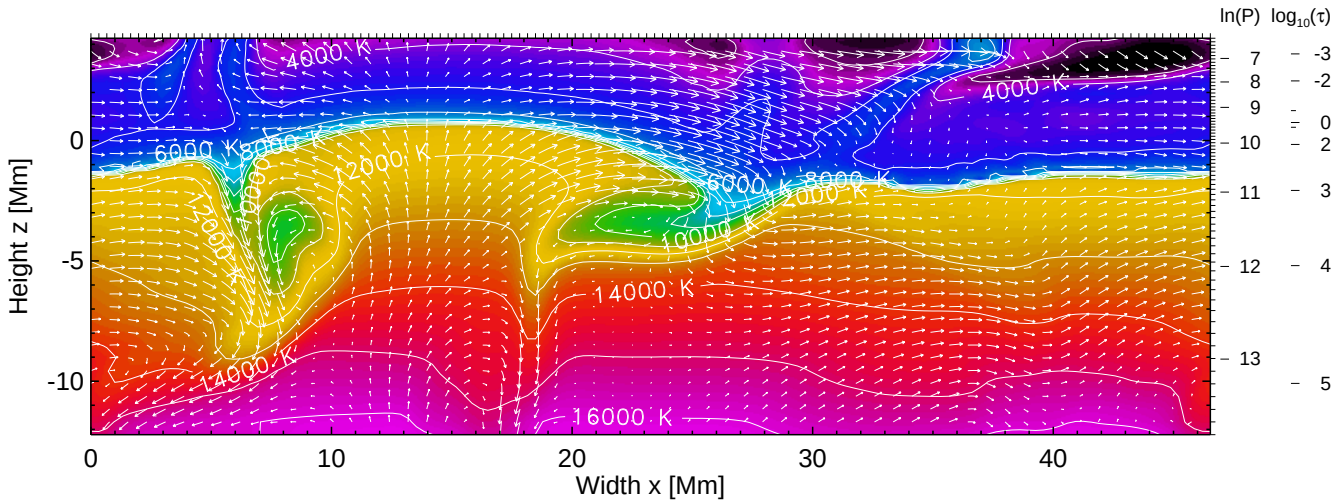

Figure 5: Snapshot of a G type star model (gt57g35n3) with $T_{\rm eff}$=5 770 K, log$g$=3.54, solar metallicity, t=117 000 s, 142×71 grid points, $v_{\rm max}$∼17.7 km/s, $F_{h,{\rm max}}$∼1 $\sigma {T_{\rm eff}}^4$. Only the upper part of the convection zone is contained in the computational volume.

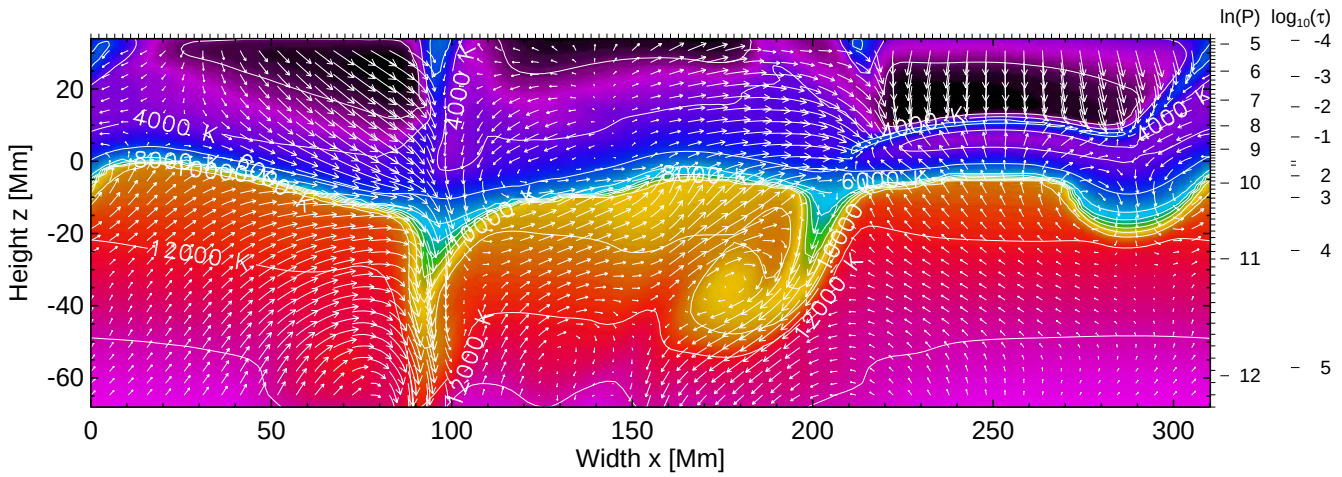

Figure 6: Snapshot of a model of a star near the base of the Red Giant Branch (gt48g25n1) with $T_{\rm eff}$=4 800 K, log$g$=2.54, solar metallicity, t=272 000 s, 142×71 grid points, $v_{\rm max}$∼11.8 km/s, $F_{h,{\rm max}}$∼1 $\sigma {T_{\rm eff}}^4$. Only the upper part of the convection zone is contained in the computational volume.

3 Scaling of the size of the granules

Solar-type convection (represented by the models in Figs. 4 to 6) shows only little scatter in the ratio between the typical horizontal size of a granule and the pressure scale height (Fig. 7, top). On the other hand, when radiation becomes more and more dominating and convection becomes less and less efficient (models in Figs. 1 to 3), there is a systematic trend with effective temperature: weaker convection is accompanied by larger granules.

Nevertheless, one can ignore these small deviations and extrapolate the scaling of the granular size with the pressure scale height towards lower surface gravities up to red supergiants with $\log g \sim 0$. It turns out, that a single granule might cover a significant fraction of the stellar surface (Schwarzschild M., 1975, ApJ 195, 137). See Fig. 7, bottom.

4 Convective and escape velocities

A shown in Fig. 8 (top panel), there is no strong dependency of the convective velocities with gravity. All solar-type convection zones have a value near 2–3 km/s. The highest velocities in the present sample are found in main-sequence F type stars ($\log g$=4.44, $T_{\rm eff} \sim$7 000 K) and in the cooler DA White Dwarfs ($\log g$=8.00, $T_{\rm eff} \sim$11 400 K). The smallest velocities have hot A type stars ($\log g$=4.44, $T_{\rm eff}$=9 000 K) and the hotter DA White Dwarfs ($\log g$=8.00, $T_{\rm eff}$=14 200 K).

The peak values lie well above the averages and for a red supergiant the peak convective velocity might come close to the escape velocity of the star. Thus, the strong mass loss of a supergiant might be due to material which is blown away from the star directly by violent convective motions. Or the matter might be pushed into regions which are cool enough to allow the formation and radiative acceleration of dust.

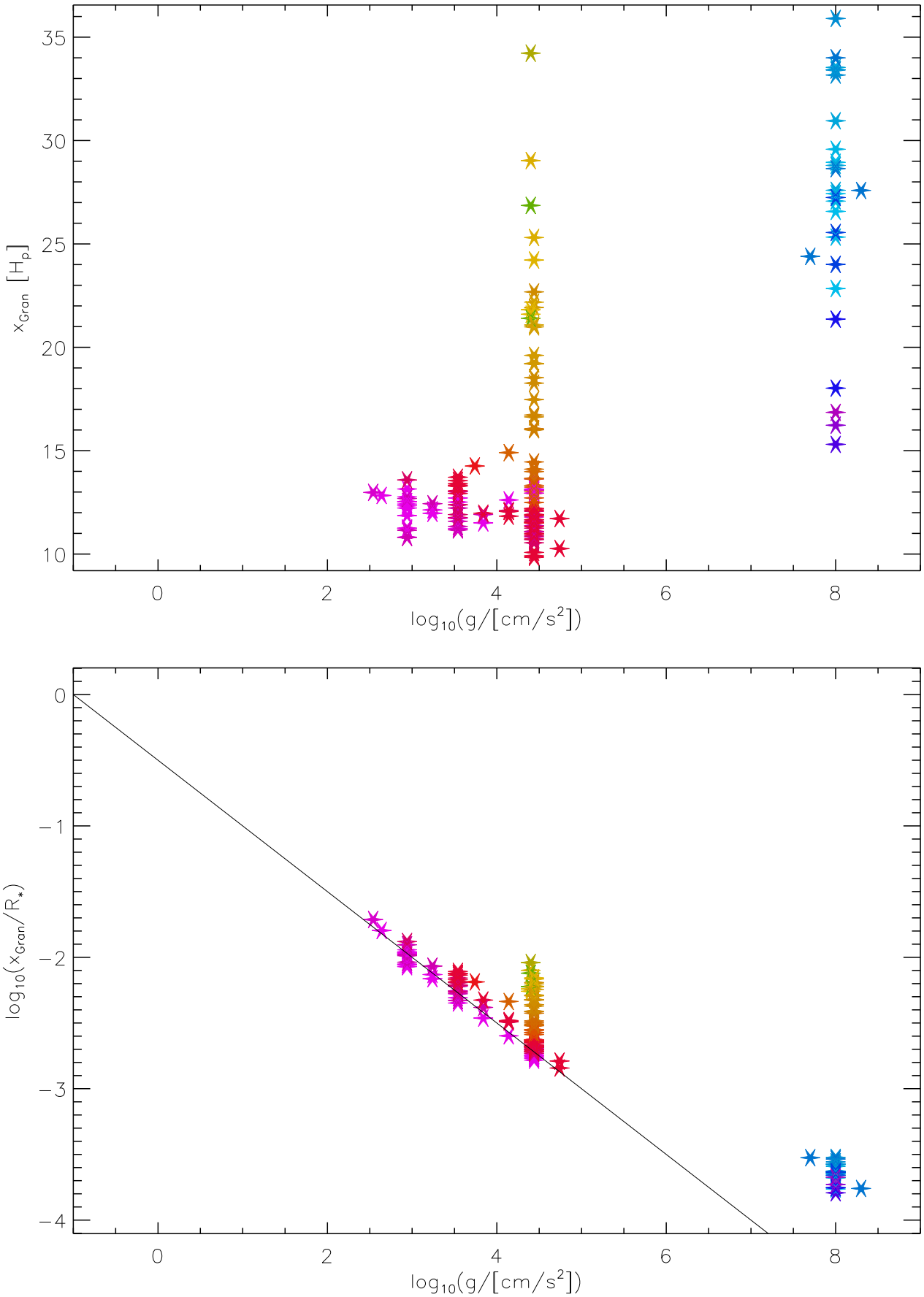

Figure 7: Upper panel: Mean horizontal extent of a granule measured in pressure scale heights at the top of the convectively unstable region versus surface gravity. Lower panel: Mean horizontal extent of a granule as fraction of the stellar radius versus surface gravity. The coloring indicates effective temperature: from $T_{\rm eff}$=4 300 K (red/violet) to 14 200 K (blue/violet). The black line marks the proportionality $x_{\rm gran}/R_* \propto g^{-1/2}$.

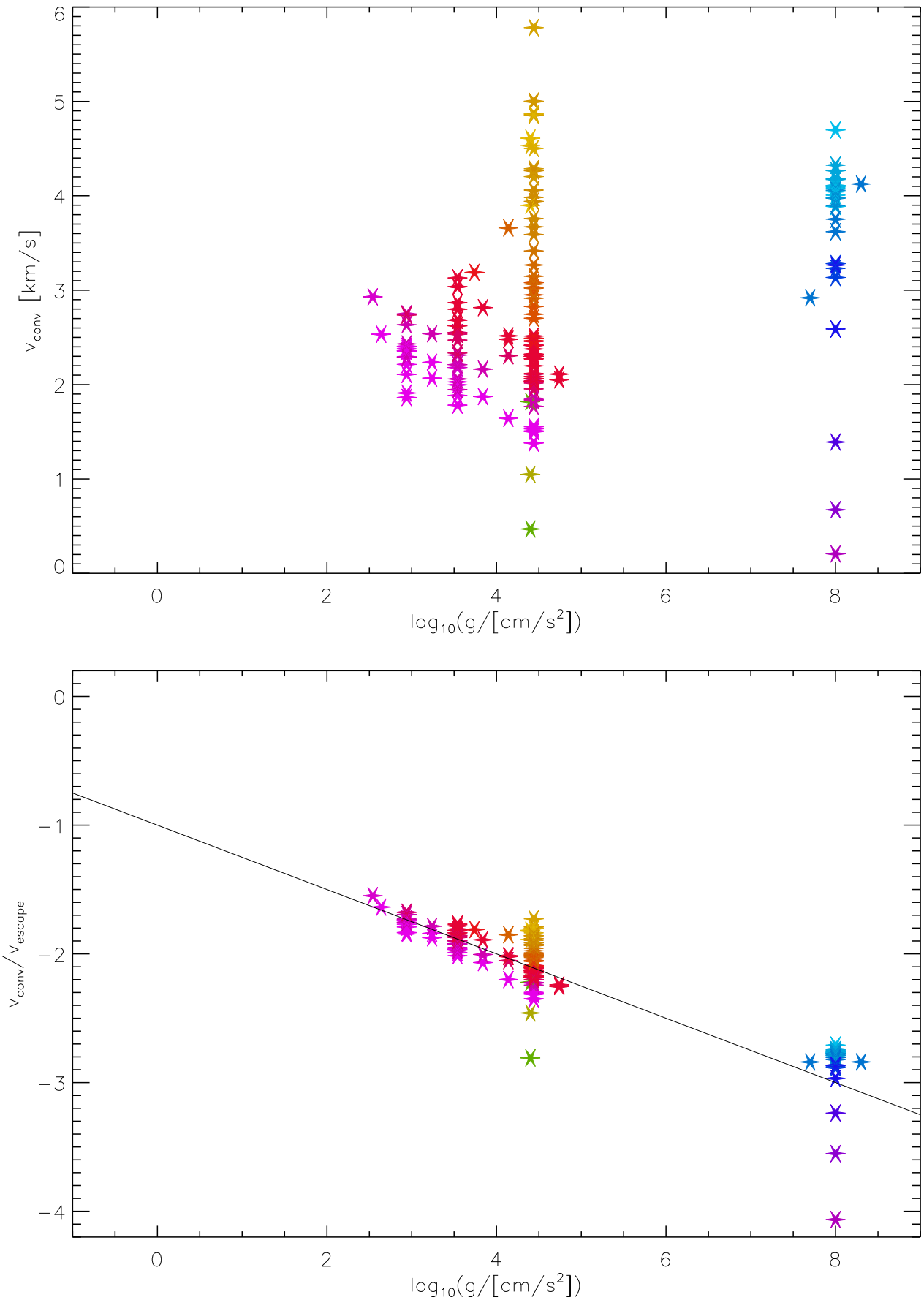

Figure 8: Upper panel: Typical vertical convective velocity versus surface gravity. Lower panel: Typical vertical convective velocity as fraction of the escape velocity at the stellar surface versus surface gravity. Color indicates effective temperature. The black line marks the proportionality $v_{\mathrm{conv}}/v_{\mathrm{escape}} \propto g^{-1/4}$.

5 Temperature gradients, opacities

While the typical horizontal extent of a granule scales well with the pressure scale height (Fig. 7), the temperature incline below the photosphere becomes steeper with decreasing surface gravity due to the variation of the temperature dependence of the opacity with density. In Fig. 9 the corresponding entropy jump is drawn for three stars separately for up and down flows.

A smaller transition region puts higher demands on the numerical resolution and/or the stability of the radiation hydrodynamics code.

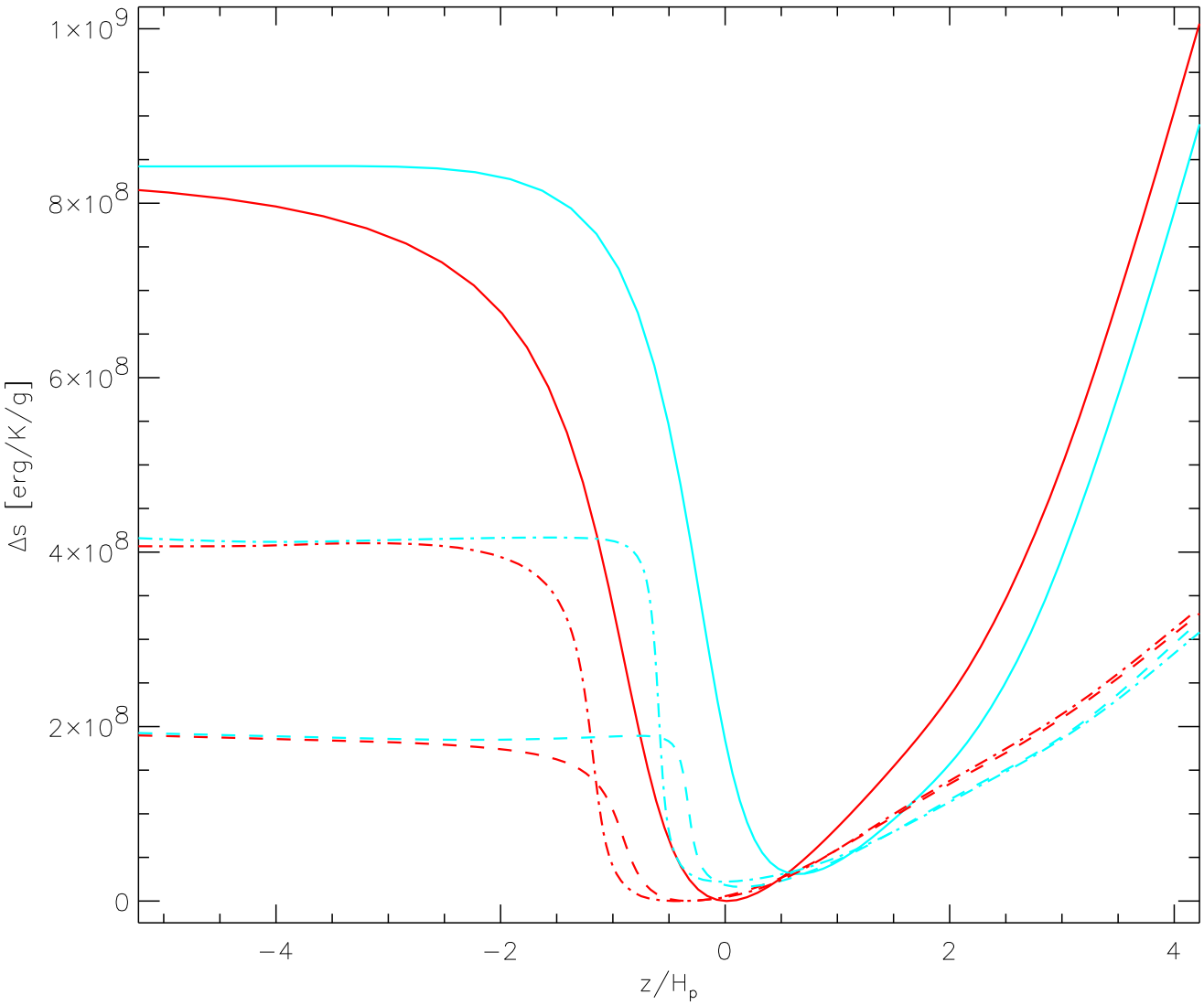

Figure 9: The entropy excess over the photospheric minimum value is plotted for three stars (dashed lines: Sun (gt57g44n9, log$g$=4.44), dash-dotted lines: star at base of Red Giant Branch (gt48g25n1, log$g$=2.54), continuous lines: DA White Dwarf (zt114g80n1, log$g$=8.00)). The blue lines mark the averages over all columns with are at τ=1 hotter than the mean (typically the columns with upward flow). The red lines mark the averages over all columns with are at τ=1 cooler than the mean (typically the columns with downward flow).

6 Supergiants

To find out how the convective envelope of a red supergiant does look like, the project "Star in a Box" has been started: With a new 3D hydrodynamics code – employing a Roe solver extended to include gravitation and ionization – the whole star is contained in the computational box with a Cartesian grid. The core of the star is omitted by smoothing out the gravitational potential.

As a preliminary result, a snapshot of an early phase of one of the first test runs is shown in Fig. 10. Large scale convective flows deform the surface of the star significantly. The model has still to be improved (e.g. the matter is still flowing towards the star because the initial settling is not yet over). However, in the end it should be possible to simulate the envelope of a red supergiant as e.g. Betelgeuse with this method.

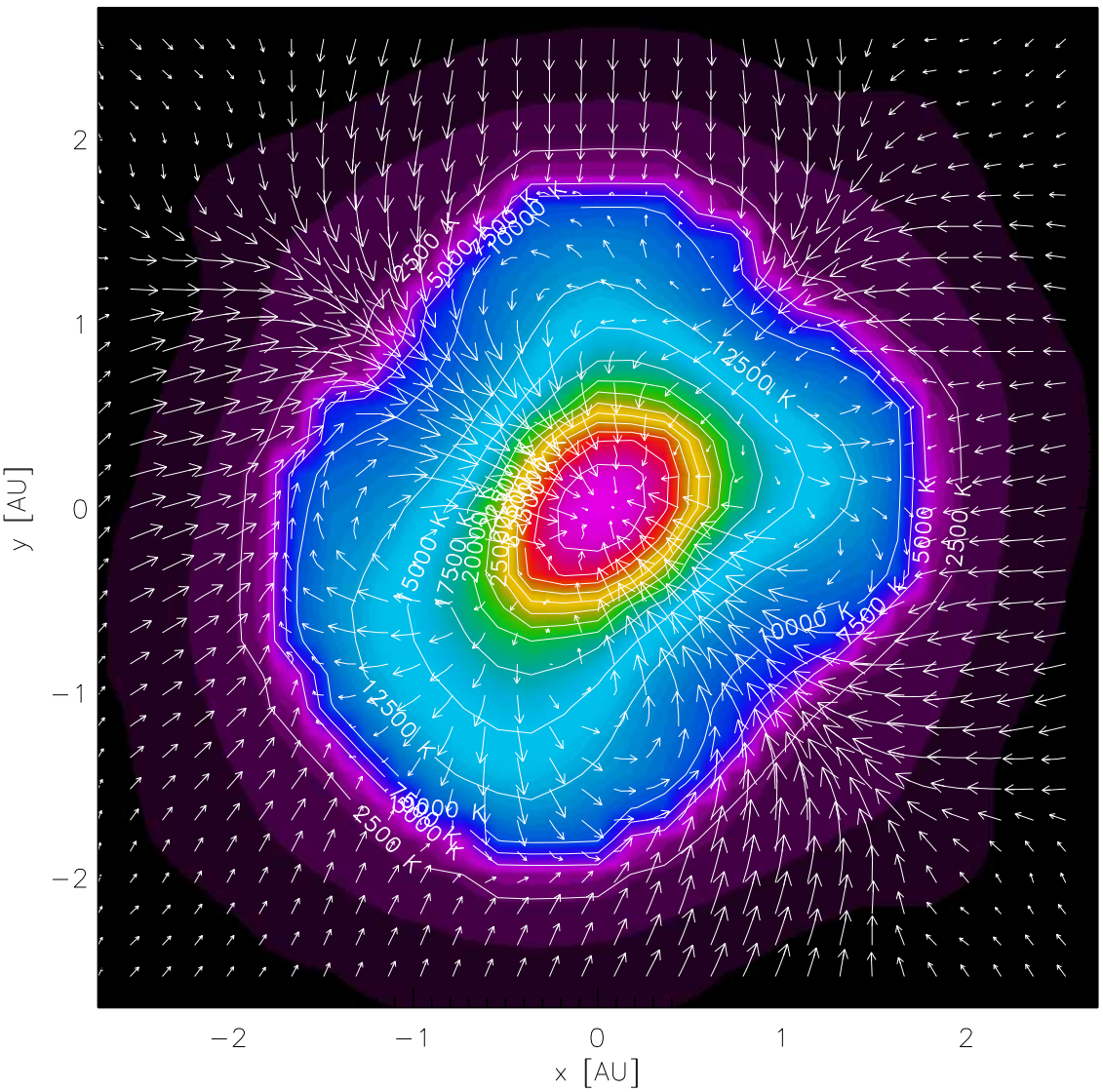

Figure 10: Slice of a 3D model of a supergiant (betelgeuse-4-2) with $M{=}1\,M_\odot$, solar metallicity, $t_{\rm int}{=}10^7$ s, $t{=}2.25\,10^8$ s, 31^3 grid points, $v_{\rm max}{\sim}6.1$ km/s.

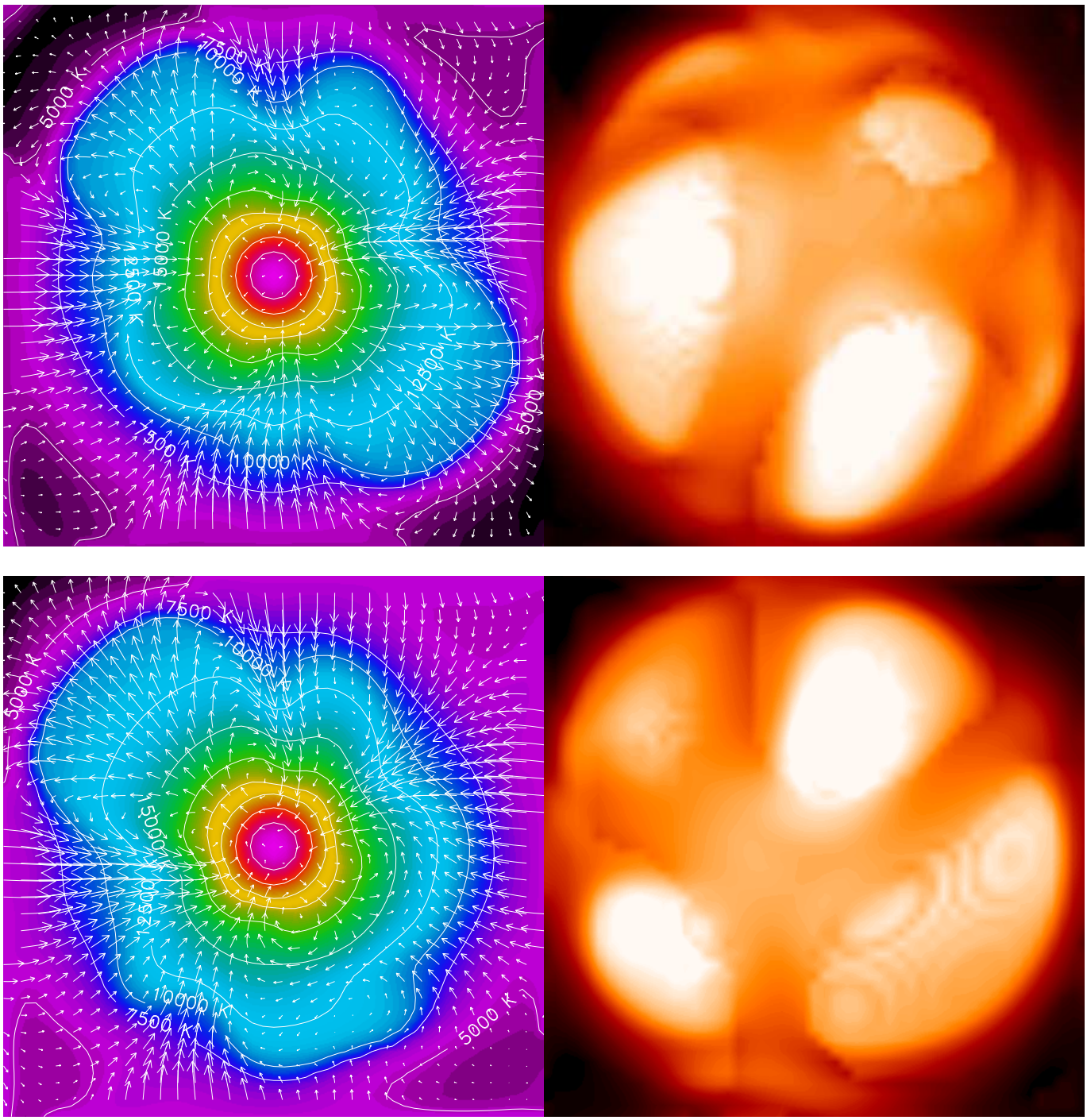

Figure 11: Left: Two slices through a scaled 3D model of a supergiant. Right: Two intensity images. 51^3 grid points.

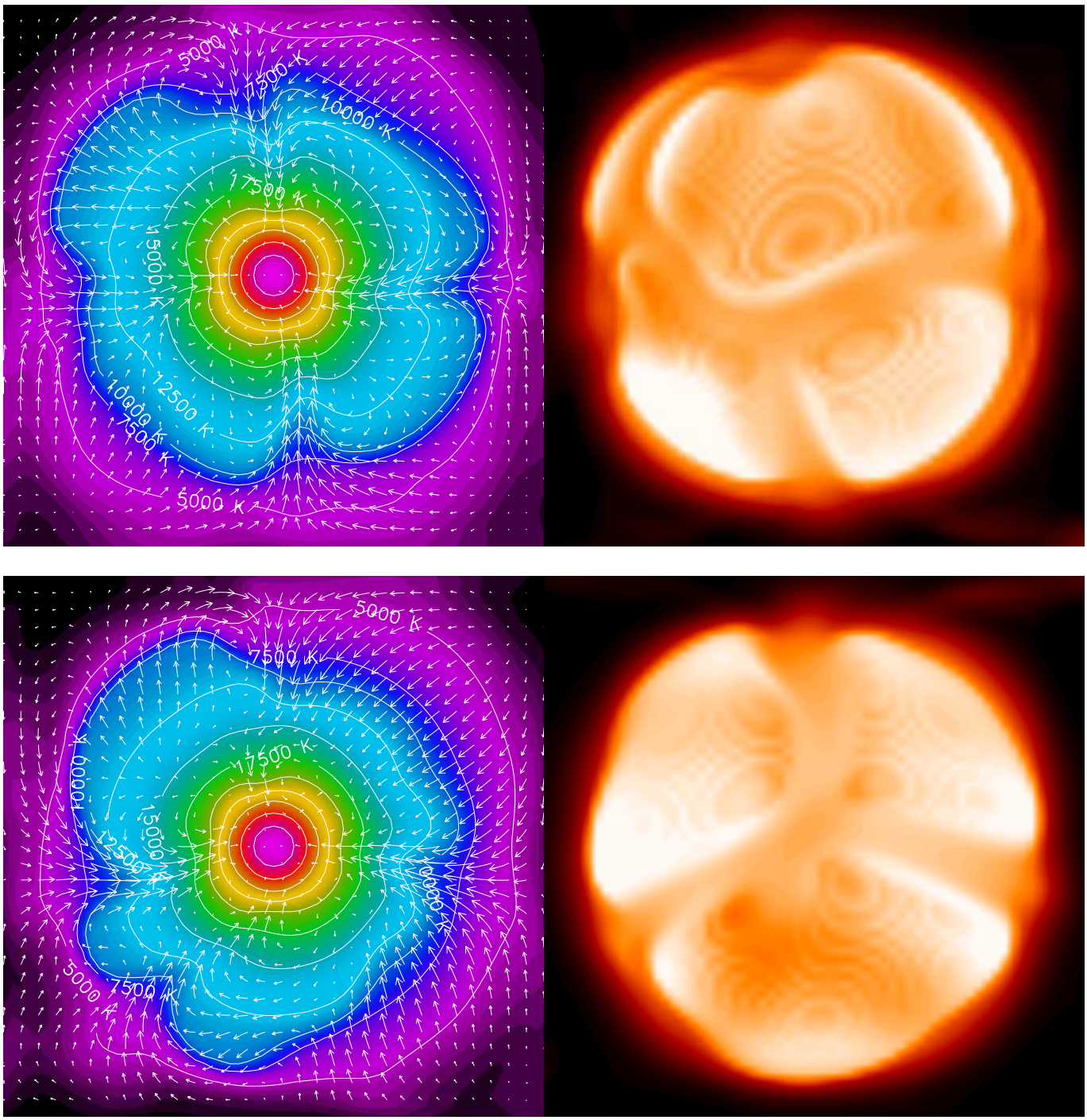

Figure 12: Left: Two slices through a scaled 3D model of a supergiant. Right: Two intensity images. 63^3 grid points.